A comparison of three methods for estimating velocity changes between time-lapse microseismic signals

Chinaemerem O. Kanu and Andrew Muñoz
Center for Wave Phenomena, Colorado School of Mines, Golden CO 80401

ABSTRACT
Time-lapse seismic signals provide information about subsurface velocity changes. The accuracy with which we measure these velocity changes is dependent on the accuracy of time shift measurements. We compare three methods of estimating time shifts using real and synthetic microseismic time-lapse signals, and use these time shifts to estimate relative velocity changes. We compare: 1) time-shift cross-correlation, 2) stretch method, and 3) smooth dynamic time warping (SDTW); SDTW provides the most detailed estimation of both time shifts and relative velocity changes among the three methods.

1 INTRODUCTION

Subsurface time-lapse velocity changes can be monitored using repeating earthquakes and microseismic events (Poupinet et al., 1984). Velocity changes might be caused by fluid injection from hydraulic activities (Davis et al., 2003), hydrocarbon migration and production (Zoback and Zinke, 2002), and stress-induced changes. Velocity changes that are weak, localized, or embedded within a noisy signal are challenging to detect. We seek a method that estimates the relative velocity changes in the presence of noise and without any prior knowledge of the subsurface velocity structure.

These velocity changes are heterogeneous and vary non-linearly with traveltime. Estimating accurate velocity changes requires that we use a high-resolution traveltime estimation method. Windowed cross-correlation (sometimes known as moving window cross-correlation) is a well known method used for estimating time shifts. Another well-known method, the stretching method, better estimates traveltimes and also directly estimates relative velocity changes. We introduce a new technique for time-lapse traveltime estimation called dynamic time warping, which is a well-known signal processing method. To compute these traveltimes, we use a modified version called smooth dynamic time warping (SDTW) (Hale and Compton, 2013). We then compute relative velocity changes from these time shifts. To compare these three methods, we to measure the time shifts between both synthetic and recorded microseismic time-lapse signals using each method and compute relative velocity changes.

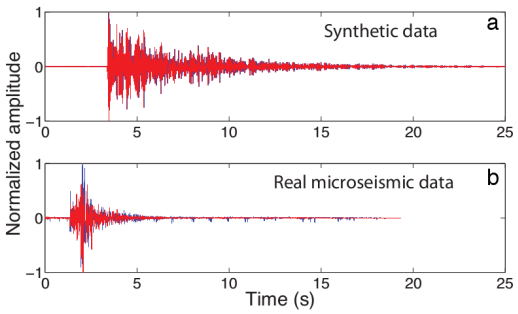

Figure 1. Synthetic time-lapse signals (a) and recorded microseismic time lapse signals (b). The blue curve is the baseline signal and the red curve is the time-lapse signal.

2 METHODS

Time-lapse velocity changes within the subsurface, like in a stimulated reservoir, induce travel time delays on seismic waves. We estimate these delays and use them to compute relative velocity changes.

2.1 Windowed cross-correlation

Windowed cross-correlation of paired signals is a common technique used for time-shift estimation. This technique has specifically been used for time shift estimation in time-lapse studies (Sens-Schönfelder and Wegler, 2006) and for computing traveltime misfits between the real data and model predicted data in geophysical inverse problems (Luo and Schuster, 1991; Van Leeuwen and Mulder, 2010). Its extensive use stems from the efficient computation cost of cross-correlation.

For a constant relative velocity change $\delta v/v$, we can

estimate the relative velocity change (Snieder, 2006)

$$\frac{\delta v}{v} = -\frac{\delta t}{t} \tag{1}$$

where δt is the traveltime change between the time-lapse seismic signals and t is the traveltime of the seismic wave.

The time shifts between the seismic codas can be estimated using the maximum cross-correlation given by

$$R(t_s) = \frac{\int_{t-t_w}^{t+t_w} d(t')\hat{d}(t'+t_s)\,\mathrm{d}t'}{\sqrt{\int_{t-t_w}^{t+t_w} d^2(t')\,\mathrm{d}t' \int_{t-t_w}^{t+t_w} \hat{d}^2(t')\,\mathrm{d}t'}}, \tag{2}$$

where $d(t)$ is the baseline coda and $\hat{d}(t)$ is the time-lapse coda. The traveltime difference δt between the two cross-correlated codas corresponds to the timeshift t_s that maximizes $R(t_s)$ (Snieder et al., 2002). The maximum cross-correlation is computed over a time window $2t_w$ centered at traveltime t. The accuracy of the relative velocity change depends on the accuracy and stability of the estimated time shifts. The estimation of time shifts is influenced by cycle-skipping, especially for large traveltime changes, while the stability of the estimated time shifts depends on the size of the cross-correlation window. Figure 2 shows the time shifts estimated from noise-free synthetic time-lapse codas using three different window sizes. By increasing the window size, the stability of the estimated time shifts increases. However, each time shift estimation is influenced by cycle-skipping, regardless of the window size. For instance, at $t = 8.2$ s in Figure 2, there is a discontinuity in the estimated time shifts. This discontinuity corresponds to a cycle-skip. The cycle-skip is solely dependent on the time shifts between the signals and the dominant period of the signals.

Time shifts between time-lapse codas can also be estimated in the frequency domain using the moving-window cross-spectrum technique (Poupinet et al., 1984). Using this technique, the time shifts δt are estimated from the phase spectrum $\phi(f)$:

$$\delta t = \frac{\phi(f)}{2\pi f}. \tag{3}$$

2.2 Stretching method

The stretching method proposed by Hadziioannou et al. (2009) provides a direct estimate of the relative velocity change $\delta v/v$ by shrinking or stretching the time-lapse coda signal relative to the baseline coda signal using an estimated stretch factor ϵ. We stretch the signals by

$$\hat{d}(\hat{t}) \rightarrow \hat{d}(t(1+\epsilon)), \tag{4}$$

where $\rightarrow$ is the stretching operation.

The estimation of the optimal stretching factor ϵ can be obtained using either the cross-correlation

$$R(\epsilon) = \frac{\int_{t_{min}}^{t_{max}} d(t')\hat{d}(t'(1+\epsilon))\,\mathrm{d}t'}{\sqrt{\int_{t_{min}}^{t_{max}} d^2(t')\,\mathrm{d}t' \int_{t_{min}}^{t_{max}} \hat{d}^2(t'(1+\epsilon))\,\mathrm{d}t'}}, \tag{5}$$

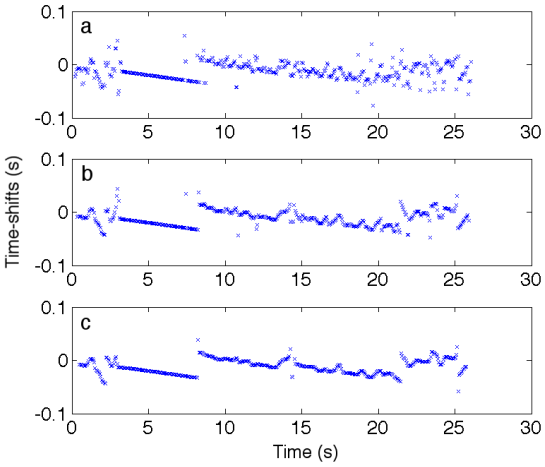

Figure 2. The stability of the windowed cross-correlation method for time shift estimation. The time shifts are estimated within time windows whose widths are relative to the dominant period T of the signal: $2t_w = 37.5T$ (a), $2t_w = 75T$ (b), and $2t_w = 112.5T$ (c), where $T = 0.033$ s.

where t_{min} and t_{max} are the minimum and the maximum traveltimes of the stretched time-lapse signals, or the L_2 norm of the difference between the time-lapse and baseline coda signals:

$$R(\epsilon) = ||\hat{d}(t(1+\epsilon)) - d(t)||_2. \tag{6}$$

The optimal ϵ is determined by the ϵ that maximizes the cross-correlation or minimizes the L_2 norm between the baseline coda and the time-lapse coda. In this study, we use the L_2 norm to pick the optimal ϵ value. This optimal stretching factor ϵ is equal to $-\delta t/t$, which, according to equation 1, is also equal to the estimated relative velocity change $\delta v/v$.

Hadziioannou et al. (2009) show, using laboratory data, that the stretching method is a more accurate and robust estimate of $\delta v/v$ compared to the window cross-correlation method. The stretching method is limited to a constant $\delta v/v$ over the window that the stretch factor is computed. To compute a time-varying $\delta v/v$, we compute the stretch factor over smaller time windows, or we use a predefined functional relationship between the stretch factor and traveltime $\epsilon = f(t)$. To use this predefined function, we must know how the relative velocity change varies along the seismic coda. By computing the stretch factors with small coda time windows (windowed stretching method), we only need to assume the stretching window length. In the windowed stretching method, the stability of the extracted stretch factors depends on the time window length relative to the dominant period of the time-lapse signals; this dependence is similar to that found with the windowed cross-correlation method. Figure 3 shows the impact of the window length on the stability of the estimated velocity changes. The stability of the estimated relative velocity changes increases

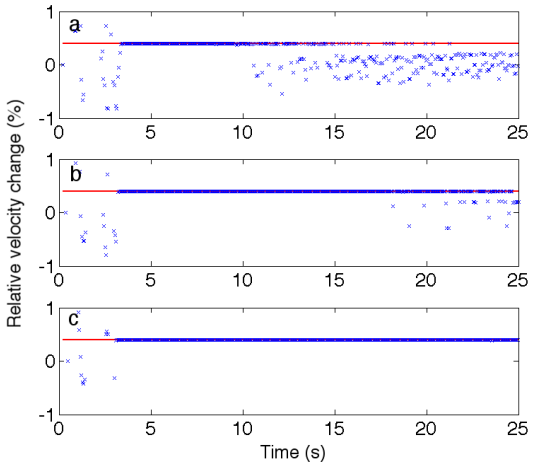

Figure 3. The stability of the windowed stretching method for relative velocity change estimation. The relative velocity changes are estimated within time windows whose widths are relative to the dominant period T of the signal: $37.5T$ (a), $75T$ (b), and $112.5T$ (c), where $T = 0.033$ s. The red line shows the exact relative velocity change.

with length of the stretching window, especially in the presence of large time shifts in the signals.

2.3 Smooth dynamic time warping

Dynamic time warping (DTW) is a widely used algorithm in speech-processing and has recently been modified and applied to geophysics (Hale, 2013; Hale and Compton, 2013; Compton and Hale, 2013). We use Hale and Compton's (2013) modified form of DTW called smooth dynamic time warping (SDTW) to compute time shifts between time-lapse signals; this modification of DTW samples time shifts at coarse intervals, which decreases the resolution of (or *smooths*) the time shifts. SDTW computes a globally optimal solution to a non-linear minimization problem (the alignment between two time-lapse signals), subject to constraints on time shifts.

Specifically, we align the baseline signal $d(t)$ to the time-lapse signal $\hat{d}(t)$ such that

$$\hat{d}(t) \approx d(t - u(t)), \tag{7}$$

where $u(t)$ are the time shifts that optimally align the time lapse signals. These shifts are subject to constraints on $\mathrm{d}u/\mathrm{d}t$. We follow the same analysis as Muñoz and Hale (2014) to relate $\mathrm{d}u/\mathrm{d}t$ to relative velocity changes:

$$\begin{aligned} \frac{\mathrm{d}u}{\mathrm{d}t} &= \frac{\hat{v}(t) - v(t)}{v(t)}, \\ &= -\frac{\delta v}{v}, \end{aligned} \tag{8}$$

where $\hat{v}$ is the velocity of the time-lapse signal, v is the velocity of the baseline signal, and $\delta v/v$ is the relative velocity change. We limit these velocity changes to constrain $\mathrm{d}u/\mathrm{d}t$:

$$\min\left(\frac{\delta v}{v}\right) \leq \frac{\mathrm{d}u}{\mathrm{d}t} \leq \max\left(\frac{\delta v}{v}\right). \tag{9}$$

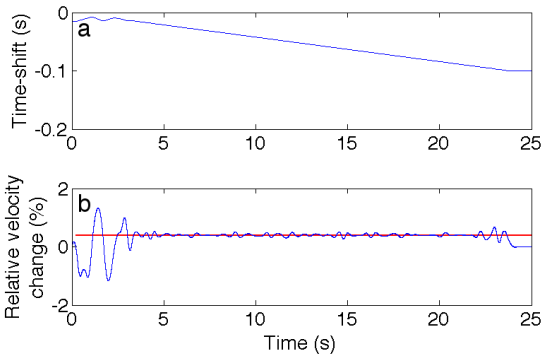

Figure 4. Time shifts and relative velocity changes estimated via SDTW. The time shifts (a) and the relative velocity changes (b) are computed from the synthetic time-lapse signals shown in Figure 1. We compare the exact velocity change (red) to the estimated relative velocity changes (blue) (b).

Following Compton and Hale (2013), we use an amplitude-aligned, non-uniform grid (computed from the baseline signal) to estimate time shifts. These grid points align with the largest amplitudes within a time window of at least 0.25 s. We show an example of these grid points in section 3. The grid spacing prevents us from sampling time shifts too finely. At the grid points, we are more confident with our time shift estimates and therefore our relative velocity change estimates compared with time shifts estimated at blindly sampled coarse grid points.

Figure 4a shows time shifts, computed using SDTW, that align the synthetic microseismic baseline and time-lapse signals shown in Figure 1, and Figure 4b shows the associated relative velocity changes in blue compared to the exact velocity changes in red. These computed relative velocity changes align well with the exact values.

A geophysically reasonable assumption is that relative velocity changes are smooth and continuous. Therefore, we interpolate time shifts between grid points using cubic splines, and because cubic splines have continuous first derivatives, our resulting relative velocity changes are are smooth. We illustrate the sensitivity of constraints computed using equation 9 in Figure 8b, where the variation in relative velocity change is larger in the late times of the time-lapse signal than at the earlier times; this instability may be attributed to the decrease in signal to noise ratio with time.

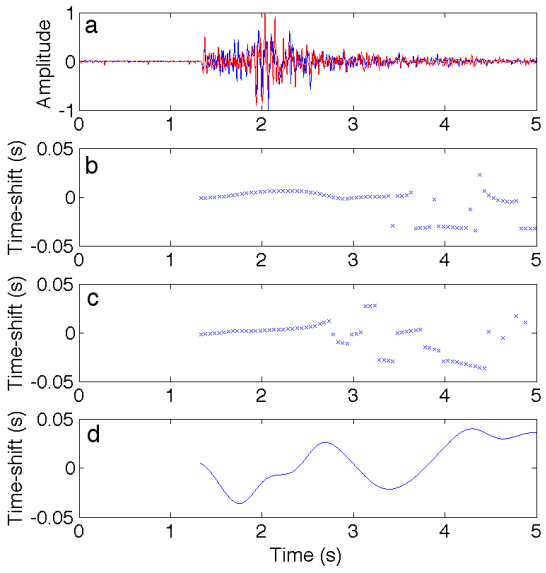

Figure 5. Time shifts computed from the unfiltered time-lapse microseismic signals (a) using windowed cross-correlation (b), the windowed stretching method (c), and SDTW (d).

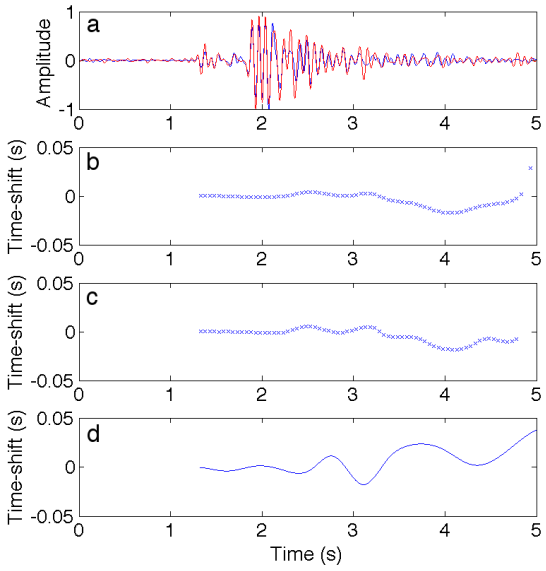

Figure 6. Time shifts computed from the 5-15Hz band-passed time-lapse microseismic signals (a) using windowed cross-correlation (b), the windowed stretching method (c), and SDTW (d).

3 REAL MICROSEISMIC SIGNALS

We use recorded time-lapse microseismic signals from a geothermal field to compare the three time shift estimation methods. These microseismic signals are shown in Figure 1; their magnitude is approximately 1.5 M_w. We anticipate a non-zero relative velocity change between the microseismic signals due to the variation in the subsurface properties over time. These recorded microseismic signals are noisy, which will affect the accuracy of the estimated time shifts and relative velocity changes (Weaver et al., 2011).

We compute these time shifts using the three previously discussed methods: windowed cross-correlation, window stretching method, and SDTW. Figure 5 shows the estimated time shifts using the full-bandwidth microseismic signals. The time shifts estimated using windowed cross-correlation and the window stretching method are computed with overlapping window sizes of 1.0 s. Computing time shifts with the overlapping windows provides a detailed estimate of the time shifts. However, this implies that the individual measurements of the time shifts are correlated. Figure 5 shows that the estimated time shifts computed using windowed cross-correlation and stretching method have less variability compared to the SDTW estimates, especially at times with high signal-to-noise ratios. This is due to an averaging effect of the windowing. Late in the coda, for example at $t > 3.5$ s, the windowed cross-correlation and stretching method show more variability in time shifts compared to the early coda. This variability in the late coda is due to the low signal-to-noise ratio; this effect is also noted when computing time shifts using SDTW, as shown in Figure 5b. However, the estimated time shifts using SDTW are more continuous. In Figures 5d and 6d, we bound $\delta v/v$ to $\pm 10\%$.

We also compute the time shifts using the filtered time-lapse signals shown in Figure 6 to improve our time shift estimates. We filter the high frequency noise from the previously shown time-lapse signals using a 5-15 Hz bandpass filter; this range spans the dominant frequencies of the signal. Figure 6 shows estimates of time shifts from these filtered signals using all three methods. These estimates contain smaller time shift variations compared to the time shifts estimated from unfiltered recorded data shown in Figure 5. The time shifts computed using SDTW show a larger variability with time compared to the time shifts estimated from windowed cross-correlation and stretching method. The averaging effect of the time windowing of the time-lapse signals via the cross-correlation and stretching methods reduces this variability of the time-shifts across the coda. However, the high variability in SDTW time shifts leads to a good signal alignment, as illustrated by Figure 7a. The estimated time shifts from these three methods are similar from $t = 1$ s to $t = 2.7$ s (Figure 6). For traveltimes greater than 2.7 s, the SDTW estimated time shifts deviate from the estimated time shifts that are

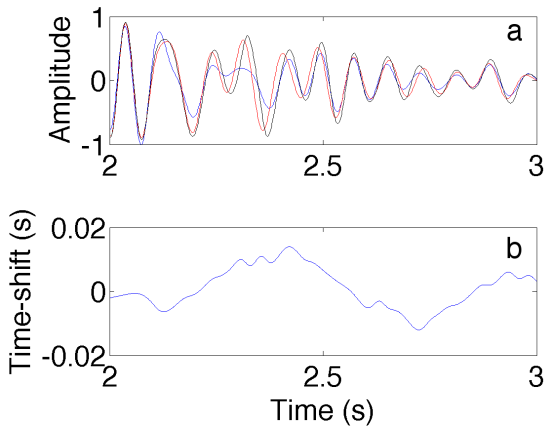

Figure 7. The 5-15Hz bandpassed time-lapse microseismic baseline signal (a) (blue), time-lapse signal (a) (red), and aligned time-lapse signal (a) (black). The time shifts (b) used to align the time-lapse signal to the baseline signal are computed using SDTW.

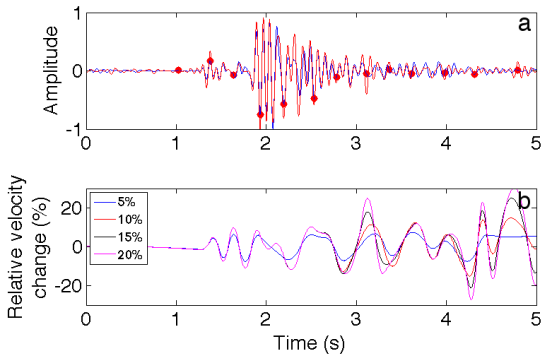

Figure 8. Relative velocity changes (b) computed from the 5-15Hz bandpassed time-lapse microseismic signals (a) using SDTW and multiple bounds on du/dt. Time shifts are sampled on an amplitude-aligned coarse grid (red points) (a).

computed using cross-correlation and stretching methods. The time shifts computed using SDTW are dependent on the sampling of amplitude-aligned grid points and the du/dt constraints used (equation 9).

From these time shifts, estimated using SDTW, we compute relative velocity changes using equation 8, as shown in Figure 8. We vary these relative velocity changes by varying the bounds on the maximum and minimum relative velocity change to: $\pm 5\%$, $\pm 10\%$, $\pm 15\%$, and $\pm 20\%$. As shown in Figure 8b, if we vary these constraints, we also vary the resulting relative velocity changes. When the signal to noise ratio is large, the relative velocity change is consistent, as seen in early times in the signal. When the signal to noise ratio is low, the relative velocity change varies more as we vary the constraints on $\delta v/v$. Figure 8 can be used to measure the time-varying uncertainty of our relative velocity change estimation. The red points shown in Figure 8a align with peaks and troughs of amplitudes in the signal. These points correspond to the grid points used to coarsely sample time shifts in SDTW. Notice a gap in grid points from 0 s to about 1 s; this is gap that we compute by measuring the first arrival time among the time-lapse signals.

4 MONITORING WITH DOWNHOLE ARRAYS

To compare the ability of these time shift estimation methods in identifying localized velocity changes within the subsurface, we consider a synthetic example with a time-lapse monitoring source (red) and receiver (blue) setup given in Figure 9a that shows both the velocity (scattering) model and the time-lapse velocity change for our monitoring problem. The velocity model is a 3-layer model with each layer having scattering properties of different statistical characteristics. The statistical characteristics of the top and the bottom scattering layers are homogeneous and structurally isotropic, while the middle layer is heterogeneous and characterizes a highly fractured reservoir. There is a 5% relative velocity change shown in Figure 9b in a black rectangle at around 3 km in depth. To measure this localized change with time-lapse signals, we use two vertical receiver arrays representing two boreholes lying on opposite sides of the localized change. These arrays record scattered waves generated by the three sources indicated by the red circle in Figure 9b. We assume acoustic wave propagation and do not account for the effect of source radiation and elastic wave modes.

Figures 10a and 10b show the time shifts and the corresponding relative velocity changes computed using the stretching method and SDTW. The estimated time shifts show similar time shift variation along the coda between methods. Similar to the time shifts estimated from the recorded time-lapse microseismic signals (section 3), the variability in the time shifts from SDTW is larger than the time shifts variations from the stretching method. This difference in the time shift variation is a function of how time shifts are estimated with each method.

Time shifts computed using STDW vary more with time compared to the windowed stretching method. Because SDTW finds the optimal alignment between two signals (subject to constraints), the computed time shifts align the microseismic signals better than the stretching method. Figure 10b also shows the time-varying relative velocity changes computed using SDTW and stretching method; SDTW shows more variability in relative velocity change with time. This estimated velocity change is a fraction of the true velocity change, where the fraction depends on the relative time

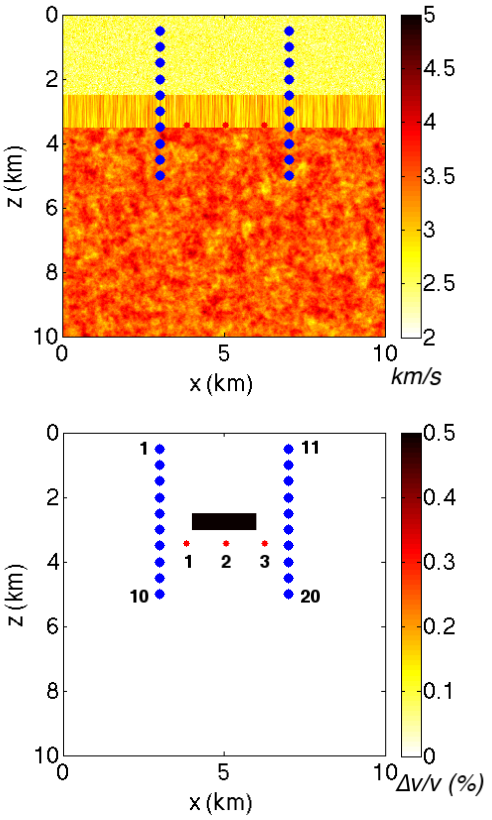

Figure 9. Numerical model for time-lapse localized velocity change. The reference velocity (scattering) model (a) with the source-receiver setup, and the exact localized velocity change (b) with the source-receiver setup.

the scattered wave spends in the region of change relative to the traveltime of the scattered wave (Planès et al., 2014).

Figure 11 shows source-receiver estimated time shifts relative to the location of the velocity change both in the early and late coda. Both time shift estimation methods give similar source-receiver distribution of the time shifts. Early in the coda waves (near $t = 1.6$ s in Figure 11a), the estimated time shifts are larger for source-receiver paths that intersect the localized velocity change. This distribution of time shifts in the early coda is also reflected in the estimated velocity changes shown in Figures 12a and 12b. Relative velocity changes computed using SDTW are a better indicator of the localized velocity change in our model than the relative velocity changes computed using the stretching method.

Later in the coda (near $t = 3.4$ s in Figure 11a), the time shifts average across the source-receiver pairs such that the source-receiver pairs below the region of change are affected by the localized change. This behavior of the time shifts in the late coda results from scattered waves that travel along paths other than the direct source-to-receiver path. We need the statistical properties of

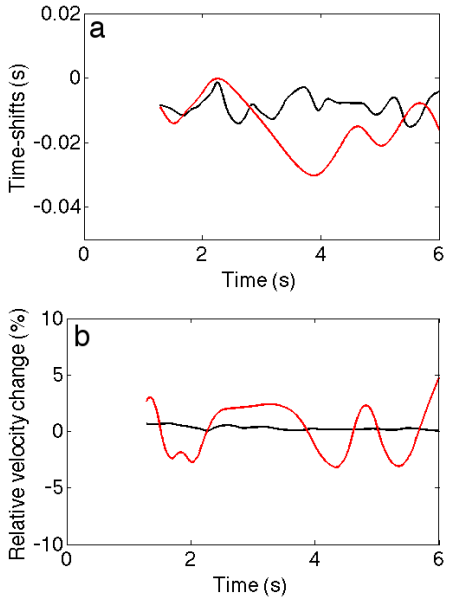

Figure 10. A comparison of the estimated time shifts (a) and relative velocity changes (b) using stretching method (black) and smooth dynamic warping (red). These timeshifts and velocity changes are estimated using the time-lapse signals for Source 2 and Receiver 3 pair shown in Figure 9.

the scattering model to understand the behavior of the time shifts and the scattered waves late in the coda. For more details on the behavior of the scattered waves in a random scattering medium, we refer the reader to Kanu and Snieder (2014). However, the time shifts in the early coda give a preliminary indication of the location of the velocity change.

5 CONCLUSION

In this paper, we compare time shift and relative velocity change estimations using three methods: time shift cross-correlation, stretching method, and smooth dynamic time warping (SDTW). We compare these methods using both synthetic time-lapse signals and recorded time-lapse microseismic signals. The synthetic signals allow for a comparison of the results of the three methods with known exact values, while the recorded microseismic signals allow us to compare the methods in the presence of noise.

Compared to the time shift cross-correlation and the stretching method, time shifts computed using SDTW are more detailed. This is because the SDTW time shifts are computed by optimally aligning two signals. In the time shift cross-correlation and stretching methods, the time shifts and relative velocity changes are estimated within windows. This leads to an averaging of the estimated time shift or velocity change values within the time window, which smooths the variations

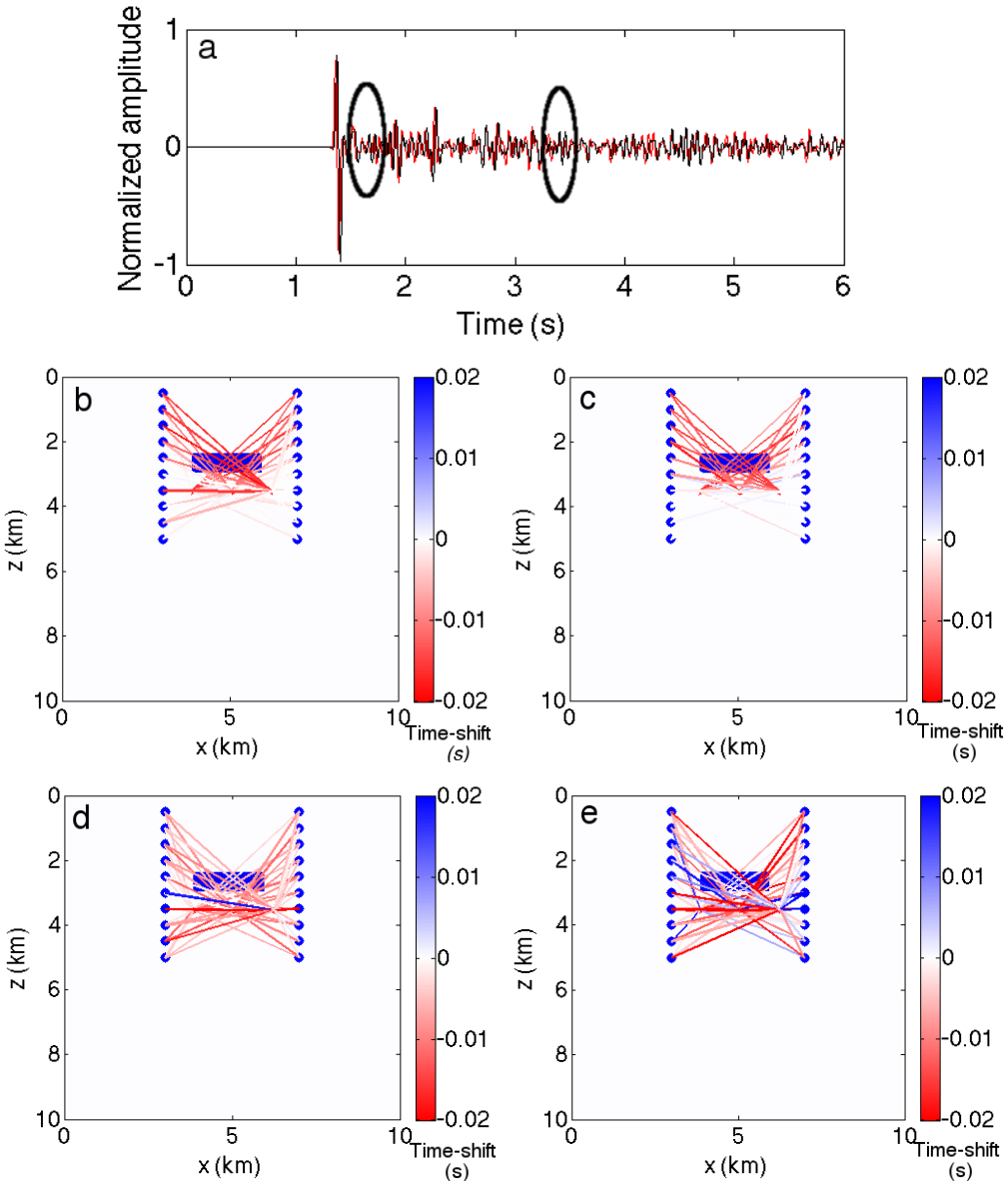

Figure 11. The early (near $t = 1.6$ s) and late (near $t = 3.4$ s) coda of the time-lapse signals (a) are highlighted. Time shifts from the early coda are computed using the stretching method (b) and SDTW (c), and time shifts in the late coda are also computed using the stretching method (d) and SDTW (e). The colored lines indicate the magnitude of the estimated traveltime changes.

in the time shifts. However, the averaging by the cross-correlation and stretching methods reduces the impact of signal noise on the time-shift estimations. SDTW may be inaccurate in the presence of noise if time shifts are computed on a finely sampled grid, but if we use an amplitude-aligned coarse grid, the effect of noise on the resulting time shifts is reduced. We are also able to constrain relative velocity changes by imposing constraints on $\delta v/v$, thus further limiting potential errors in our time shifts due to noise. We use the amplitude-aligned grid points and constraints on relative velocity changes that minimize the effect of noise and provide an optimal tie of the time-lapse signals. SDTW is also unaffected by cycle-skipping, which causes errors in estimating time shifts using the cross-correlation and the stretching methods.

ACKNOWLEDGMENTS

We thank the sponsors of the Consortium Project on Seismic Inverse Methods for Complex Structures, whose

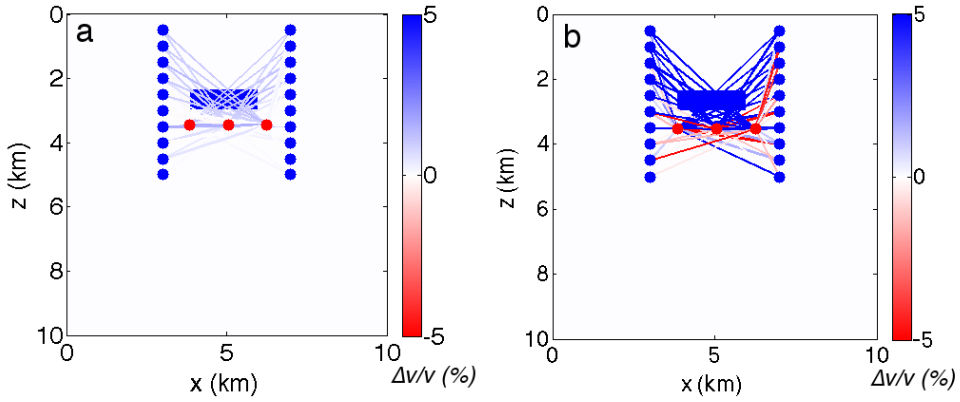

Figure 12. Distribution of the relative velocity changes between time-lapse signals computed using the stretching method (a) and SDTW (b) among source-receiver pairs. The velocity changes are estimated using the early part of the time-lapse coda. Blue circles are the receivers while the red circles are the sources. The blue rectangle gives the localized time-lapse velocity change of 5%. The colored lines indicate the magnitude of the estimated relative velocity changes.

support made this research possible. We are also grateful to Roel Snieder for initiating the idea of this study, his helpful suggestions, and his witty jokes.

REFERENCES

Compton, S. and D. Hale, 2013, Estimating v_p/v_s ratios using smooth dynamic image warping: Center for Wave Phenomena, **765**, 211–222.

Davis, T. L., M. J. Terrell, R. D. Benson, R. Cardona, R. R. Kendall, and R. Winarsky, 2003, Multicomponent seismic characterization and monitoring of the CO_2 flood at Weyburn field, Saskatchewan: The Leading Edge, **22**, 696 –697.

Hadziioannou, C., E. Larose, O. Coutant, P. Roux, and M. Campillo, 2009, Stability of monitoring weak changes in multiply scattering media with ambient noise correlation: Laboratory experiments: Journal of the Acoustical Society of America, **125**, 3688–3695.

Hale, D., 2013, Dynamic warping of seismic images: Geophysics, **78**, S105–S115.

Hale, D. and S. Compton, 2013, Smooth dynamic warping: Center for Wave Phenomena, **764**, 201–210.

Kanu, C. and R. Snieder, 2014, Numerical computation of the sensitivity kernel for time-lapse monitoring with multiply scattered waves: Center for Wave Phenomena, **816**, 291–306.

Luo, Y. and G. T. Schuster, 1991, Wave equation traveltime inversion: GEOPHYSICS, **56**, 645–653.

Muñoz, A. and D. Hale, 2014, Automatic simultaneous multiple-well ties: Center for Wave Phenomena, **788**.

Planès, T., E. Larose, L. Margerin, V. Rossetto, and C. Sens-Schönfelder, 2014, Decorrelation and phase-shift of coda waves induced by local changes: multiple scattering approach and numerical validation: Waves in Random and Complex Media, 1–27, doi:10.1080/17455030.2014.880821.

Poupinet, G., W. L. Ellsworth, and J. Frechet, 1984, Monitoring velocity variations in the crust using earthquake doublets: An application to the Calaveras fault, California: Journal of Geophysical Research, **89**, 5719–5731.

Sens-Schönfelder, C. and U. Wegler, 2006, Passive image interferometry and seasonal variations at Merapi volcano, Indonesia: Geophys. Res. Lett., **33**, L21302, doi:10.1029/2006GL027797.

Snieder, R., 2006, The theory of coda wave interferometry: Pure and Applied Geophysics, **163**, 455–473.

Snieder, R., A. Grêt, H. Douma, and J. Scales, 2002, Coda wave interferometry for estimating nonlinear behavior in seismic velocity: Science, **295**, 2253 –2255.

Van Leeuwen, T. and W. A. Mulder, 2010, A correlation-based misfit criterion for wave-equation traveltime tomography: Geophysical Journal International, **182**, 1383–1394.

Weaver, R. L., C. Hadziioannou, E. Larose, and M. Campillo, 2011, On the precision of noise correlation interferometry: Geophysical Journal International, **185**, 1384–1392.

Zoback, M. and J. Zinke, 2002, Production-induced normal faulting in the Valhall and Ekofisk oil fields: Pure and Applied Geophysics, **159**, 403–420.